V European Conference on Computational Fluid Dynamics
ECCOMAS CFD 2010
J. C. F. Pereira and A. Sequeira (Eds)
Lisbon, Portugal, 14–17 June 2010

EFFECT OF VERTICAL TRANSLATION ON UNSTEADY AERODYNAMICS OF A HOVERING AIRFOIL

Erkan Gunaydinoglu[*] and D. Funda Kurtulus[†]

[*]Department of Aerospace Engineering, Middle East Technical University
06531 Ankara, Turkey
e-mail: gunaydin@ae.metu.edu.tr

[†] Department of Aerospace Engineering, Middle East Technical University
06531 Ankara, Turkey
dfunda@ae.metu.edu.tr

Key words: Flapping flight, Micro Air Vehicles, Hover, Figure of Eight

Abstract. *In this study, the unsteady aerodynamics of SD7003 airfoil undergoing "figure-of-eight" motions with vertical translation amplitudes of 0c (normal hover), 0.5c and 1c is investigated numerically. The forces and vortex fields are compared at the same Reynolds number that is defined with respect to the maximum absolute velocity. Also the effect of the reduced frequency is investigated and it is found that in the meantime, decreasing reduced frequency and increasing Reynolds number does not alter the general force and vortex-field trends but increases the peaks in the aerodynamic forces for same motion.*

1 INTRODUCTION

The flapping flight has attracted biologists and physicists more than a century to be capable of understanding the nature's choice and mimicking that choice for development of successful micro aerial vehicles. In spite of the remarkable interest on the topic, a precise theoretical and computational analysis is not available yet due to the complexity of the motion. This complexity could be simplified by using airfoils in pitch, plunge and ramp motions. Wang [1] showed that the two-dimensional analysis is a reliable tool for investigation of flapping flight by emphasizing the agreement of her results with the results of Hall et al. [2]. Freymuth [3] studied the thrust generation of a hovering airfoil and identified three types of motions; normal hovering mode, water treading mode and oblique mode. He showed that the vertical signature of hovering thrust is the reverse Karman vortex street with a character of jet stream. The thrust generation of a sinusoidally plunging airfoil in forward flight was first shown a century ago [4-5]. Pesavento et al. [6] solved the Navier-Stokes equations around a 2D ellipse and optimized the flapping motion that needs less power required than optimal steady flight. Rather than specific studies Lehmann [7], Platzer and Jones [8], Wang [9] and Sane [10] have offered reviews on flapping wing aerodynamics for different point of views.

In this study, SD7003 airfoil undergoing "figure-of eight" and "normal hover" modes is investigated numerically. The non-dimensional vorticity contours are visualized and aerodynamic forces are calculated for different Reynolds numbers and reduced frequencies.

2 METHOD

2.1 Kinematics

Three different kinematics such as "mode A", "mode B" and "mode C" are considered. The "normal hover" mode, which is denoted as mode A in this study, is defined by Freymuth [3]. The "mode A" motion is defined as the superposition of unsteady variation of linear translation and angular rotation of an airfoil. Combining the vertical translation with the normal hover mode will result as "figure-of-eight motion". The translation motion of the airfoil is defined as a Lissajous curve, which is the graph of a set of parametric equations. Moreover, the pitching motion is defined with respect to the quarter chord location having a pitching amplitude of $\pi/2$. The pitching amplitude is adjusted to have 0° at the half of the linear translational motion in order not to have massive leading- and trailing edge vortices at this part of the flow-field. The only massive leading edge and trailing edge vortices are generated at the beginning and end of the strokes. Therefore, it will be easier to identify the vortices generated dominantly by vertical translational motion. The resulting kinematics is given by following equations:

$$x(t) = 2c\sin(\omega t + \pi/2) \tag{1}$$

$$y(t) = Yc\sin(2\omega t) \tag{2}$$

$$\alpha(t) = \pi/2 + \pi/2\sin(\omega t) \tag{3}$$

where ω is circular frequency ($\omega = 2\pi f$), f is oscillation frequency, x and y are the linear and vertical coordinates of the quarter chord location of the airfoil, α is the pitch angle with respect to the horizontal axis and Y is the amplitude of vertical translation.

The main purpose of this study is to investigate the effect of vertical translation amplitude (Y) to the hovering aerodynamics. To achieve this, three different values of Y is used in this study including normal hover mode (see Fig. 1). For the mode B motion, the vertical translation amplitude is Y=1/2 and for mode C the vertical translation amplitude Y is chosen to be 1. The resulting path of the airfoil for three modes of hovering is given in Fig. 1.

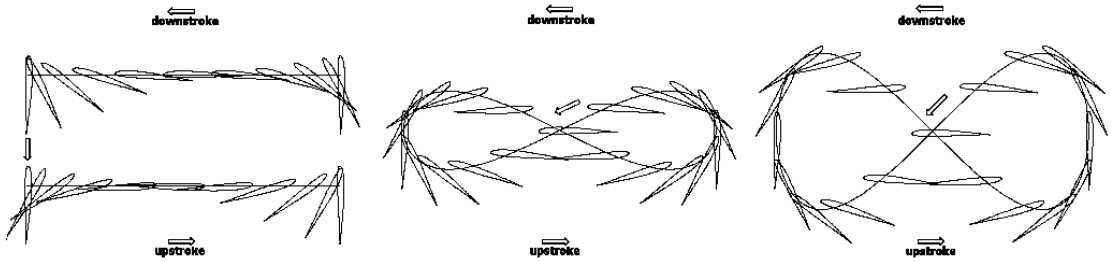

Figure 1: Position of the airfoil with time for mode A (left), mode B (middle) and mode C (right)

2.2 Solver

The two-dimensional, unsteady Navier-Stokes equations for the flow-field around SD7003 airfoil undergoing three different modes of hovering were solved via commercial CFD package Fluent 6.3. For the spatial discretization second-order upwind scheme is used. The hovering motion of the airfoil was modeled by using dynamic mesh feature of the code that is moving the whole grid as a rigid body and not deforming the grid. The dynamic mesh feature limits the unsteady formulation to the first order in time.

2.3 Grid and Time-step Refinement

The spatial and temporal sensitivity tests are performed to be sure that we have a grid and time-step independent solution. For grid sensitivity, two structured O-type grids with 199x100 and 399x200 elements are compared. These two grid domains are used to solve the flow-field around the airfoil undergoing "mode C" hovering and the resulting lift and drag coefficients are shown in Fig. 2. It is found that the grid domain with 199x100 elements is fine enough to have grid independent solution. Same procedure for time-step refinement is also performed for $T/\Delta t$ = 200, 400 and 800 and found that 400 time-steps per a period is sufficiently refined where T is the motion period and Δt is the time step.

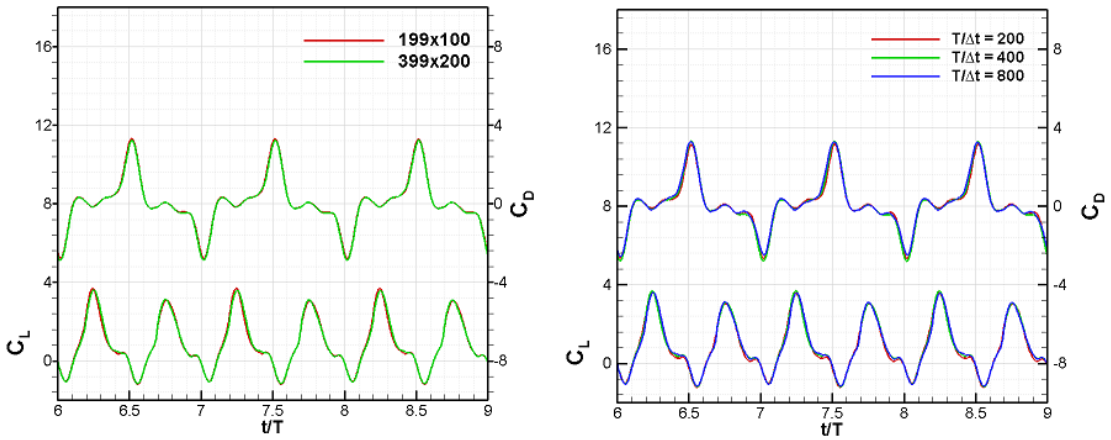

Figure 2: Time history of C_L and C_D with different grid domains (left) and with different time-steps (right) for Mode C hovering

3 RESULTS

The periodicity in terms of forces, moments and vortex-field is achieved at the sixth period for all investigated cases but here we used the solutions of the 9th period. The two important similarity parameters in regarding to the fluid dynamics of flapping motion are Reynolds number (*Re*) and reduced frequency (*k*) for which the definitions are given by eqns. (4-5):

$$Re = U_{ref}c/\upsilon \tag{4}$$

$$k = \frac{\omega c}{2U_{ref}} \tag{5}$$

In normal hover mode (mode A), the reference velocity is defined as maximum horizontal plunging velocity, $\omega c = 2\pi f c$. For "figure-of-eight" motion ("mode B" and "mode C") maximum absolute velocity (U_{ref}) is taken into account for definitions of the Reynolds number and aerodynamic force coefficients. Reynolds number for "mode A", "mode B" and "mode C" is taken as 1000. Moreover two additional cases (mode B_2 with Re=1120 and mode C_2 with Re=1415) at constant reduced frequency, k=0.25, are also investigated. Figs. 3-5 show the non-dimensional vortex-fields for "mode A", "mode B" and "mode C" respectively. The vorticity is non- dimensionalized with U_{ref}/c and consequently, the results could be compared quantitatively.

For "mode A", the airfoil is moving with zero geometric angle of attack during at about 40% of its period and at these time interval we e generation of massive separation is not expected. At the beginning of the downstroke (t/T=8.0) a LEV, that is generated at the end of previous cycle (at t/T~7.95), is observed. The airfoil hits the LEV and the low pressure area sticks to the airfoil, resulting a decrease in lift up to t/T=8.15. After that instant until t/T=8.4 the airfoil translates without any separation and lift increases up to steady state limits. Due to the symmetry of the motion same process occurs during t/T=8.5 to t/T=9.0 with opposite rotating vortices. There is a perfect symmetry in lift and drag forces for two strokes. Hence it is observed that the asymmetry of airfoil has negligible effect on the flow-field for that motion. The "mode A" stands as a base for the comparative study.

The vortex-field for "mode B" is shown in Fig.4 and the forces are shown in Fig. 6. In that motion, the amplitude of vertical translation is c/2 for which the horizontal translation amplitude is 2c. In that case, the perfect symmetry of the flow- field is lost due to the asymmetry of the airfoil which affects the vortex structures. At t/T=8.0 the onset of a LEV and TV could be observed in Fig. 4. Rather than "mode A", this time airfoil does not hit the detached LEV and TV (at t/T=8.1) and so the lift coefficient has in an increasing trend. At the beginning of the downstroke (t/T=8.0) the high suction region on the lower surface results as drag in negative direction (to the left). In contrast, at the beginning of the upstroke (t/T=8.5) the newly generated vortices creates a high suction region on the upper surface which will result a positive drag (to the right). Different than "mode A" hovering, here at t/T= 8.0 and 8.5 y-velocity is at its maximum value of $\dot{y}(t) = c\cos(2\omega t)$ and that velocity washes out the generated LEV and TV from the airfoil surface. This stretching phenomenon could be observed in Figs. 3-4 at instances t/T=8.0 and 8.5.

Fig. 6 shows the vortex-field for "mode C" hovering for which the vertical translation amplitude is 1c. At t/T=8.0 the detached LEV and TV structures are observed. These vortices are generated at t/T=7.7 and left the surface at t/T=7.8. The maximum horizontal velocity occurs at the middle of the strokes and with increasing x-velocity at t/T=8.25 and 8.75 where the airfoil has its maximum lift coefficient.

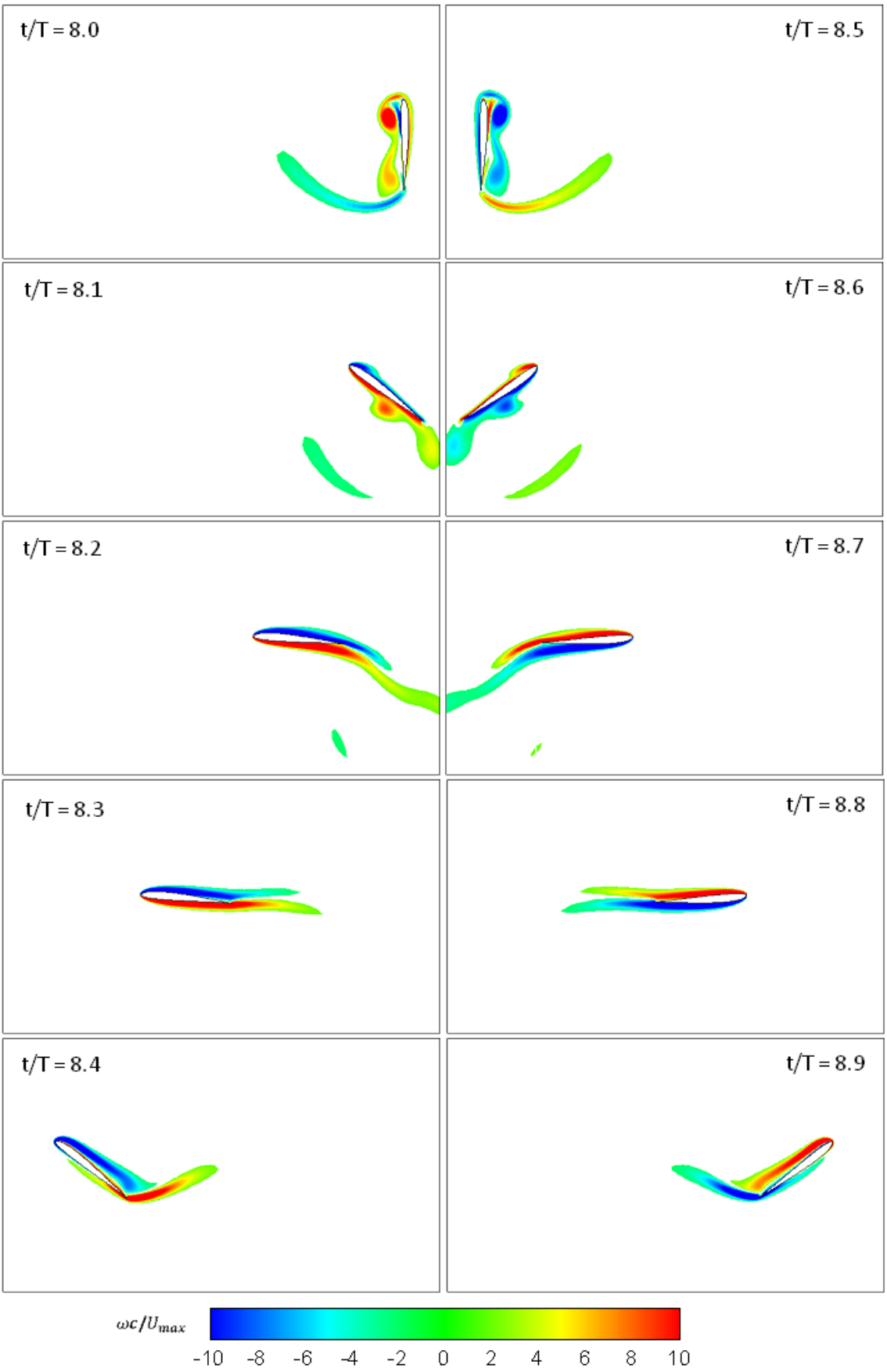

Figure 3: Non-dimensional vorticity contours for one period of "mode A" hovering at Re=1000. Red areas denote positive vorticity (CCW swirling) and blue areas denote negative vorticity (CW swirling).

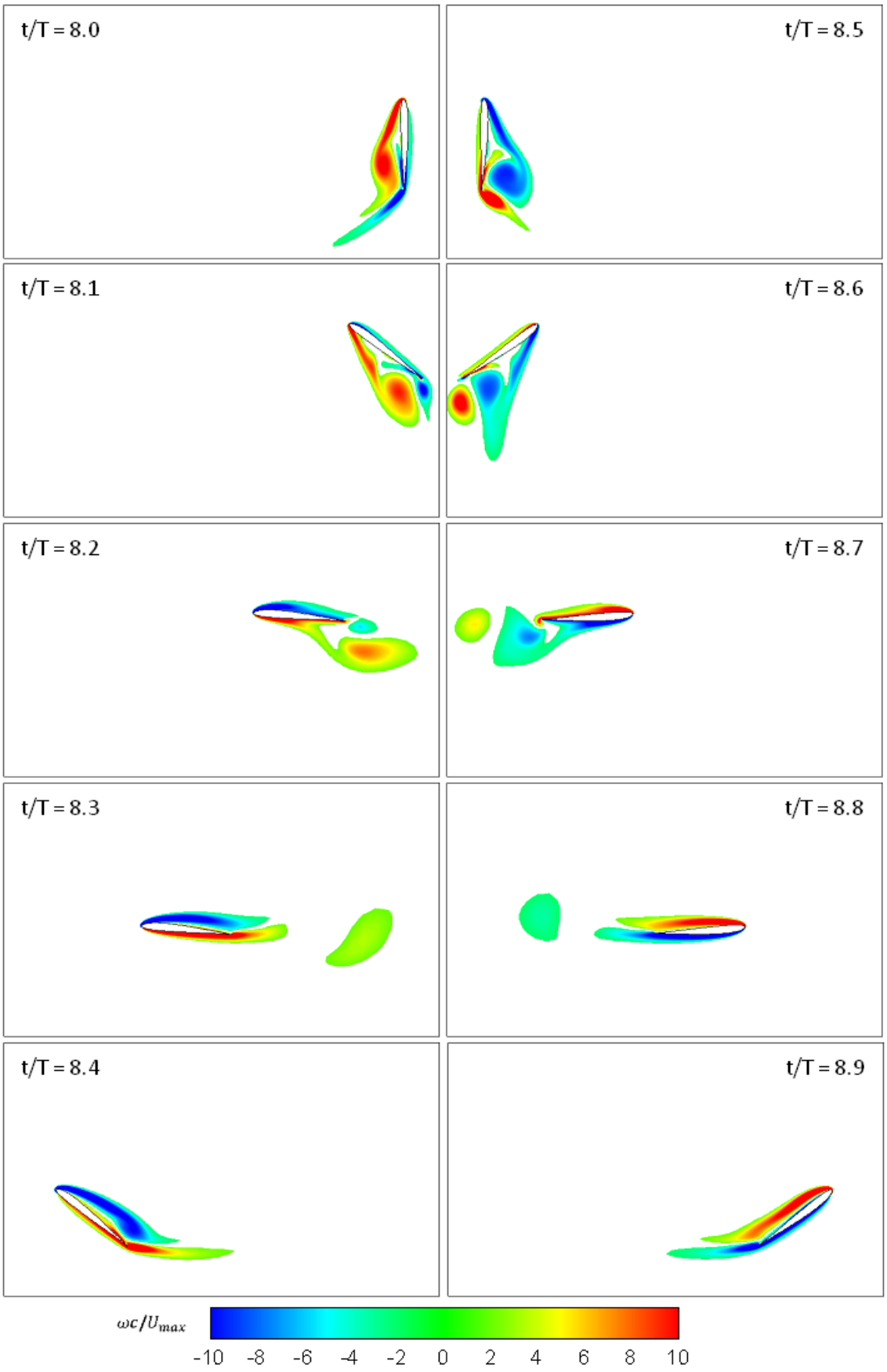

Figure 4: Non-dimensional vorticity contours for one period of "mode B" hovering at Re=1000. Red areas denote positive vorticity (CCW swirling) and blue areas denote negative vorticity (CW swirling).

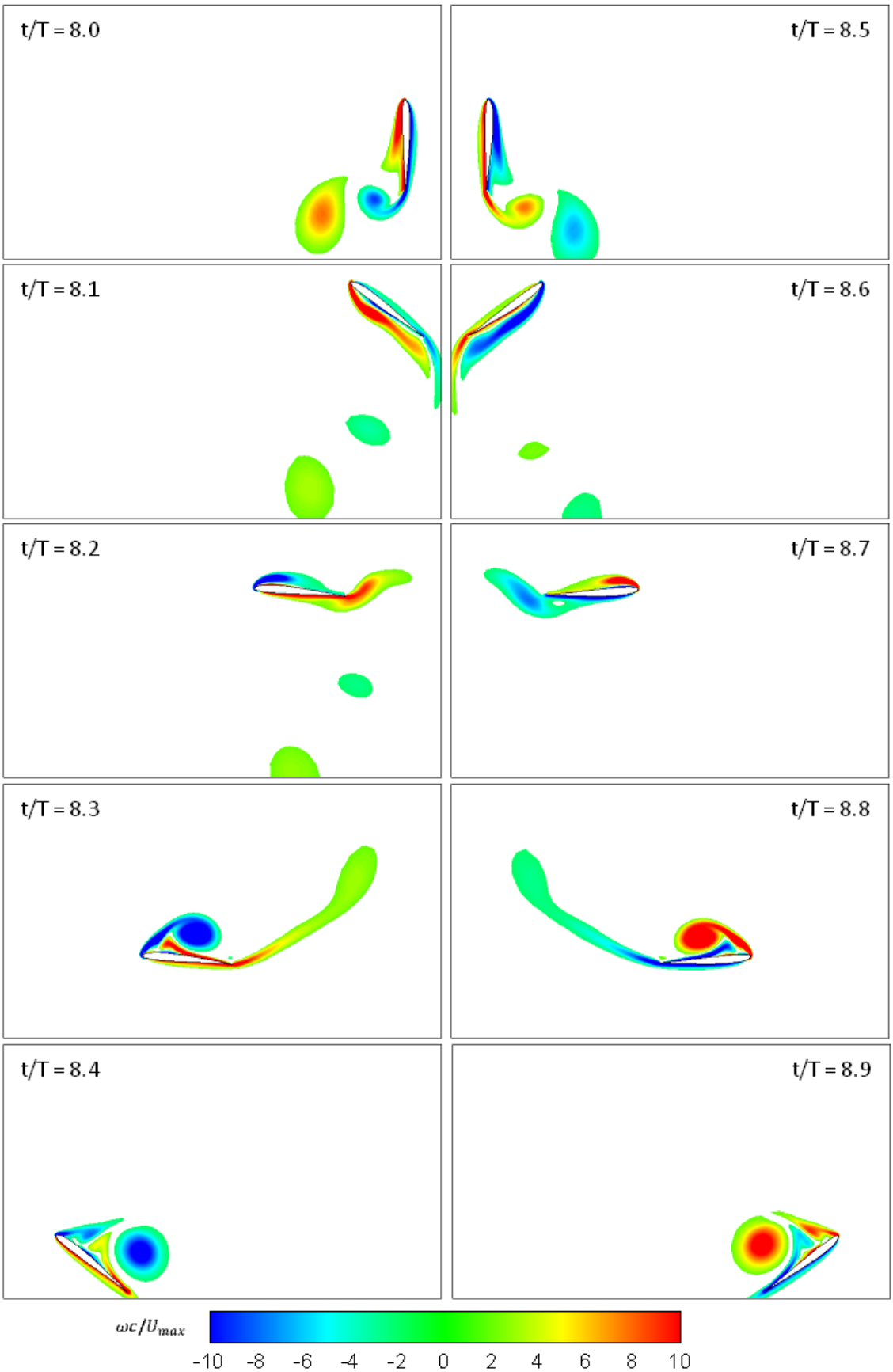

Figure 5: Non-dimensional vorticity contours for one period of mode C hovering at Re=1000. Red areas denote positive vorticity (CCW swirling) and blue areas denote negative vorticity (CW swirling).

Moreover “mode C” hovering is the only case in this study for which the detachment of vortices is occurring at the middle of the strokes. A slight difference between two strokes is observed in forces and vortex-fields in this mode rather than having perfect symmetry. The peaks of drag forces are observed at the beginning of the upstroke (t/T=8.5) and the downstroke (t/T=8.0) with a value of C_d=1.6. Since the vertical velocity of mode C is double of the mode B, it is observed that the maximum C_d value is larger than the value achieved at “mode B”.

The same study is performed for two additional cases (mode B_2 and mode C_2) for which the same chord and frequency with normal hover mode are selected. These cases are studied to see what will be done if vertical motion is added to a normal hovering system without changing any other parameters. The resulting Reynolds numbers for mode B_2 and mode C_2 are Re=1120 and Re=1415 respectively.The resulting forces are compared with other cases in Fig. 6.

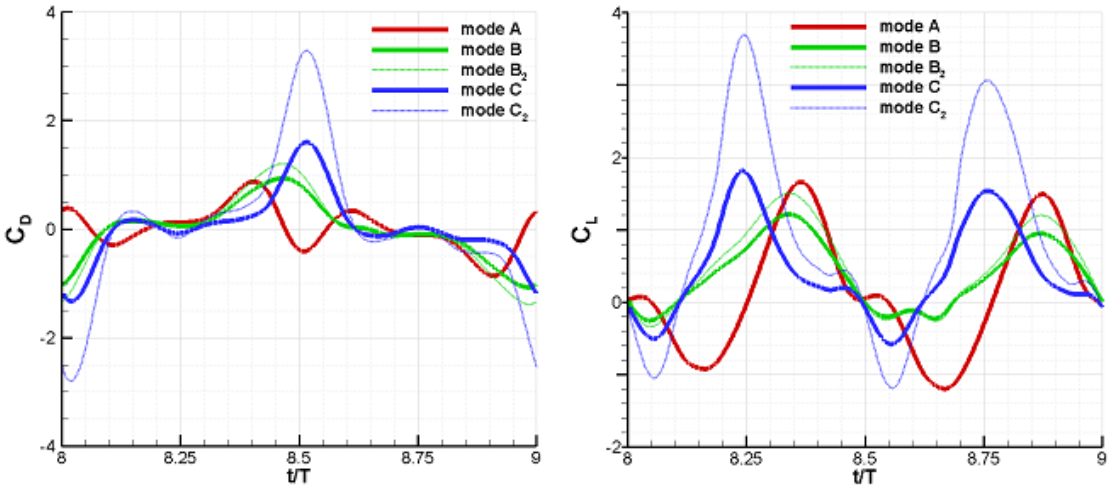

Figure 6: Time histories of C_d (left) and C_l (right) for all hovering cases studied. The solid lines denote the cases at same Reynolds number of 1000. The dashed lines denote the cases with constant reduced frequency of 0.25.

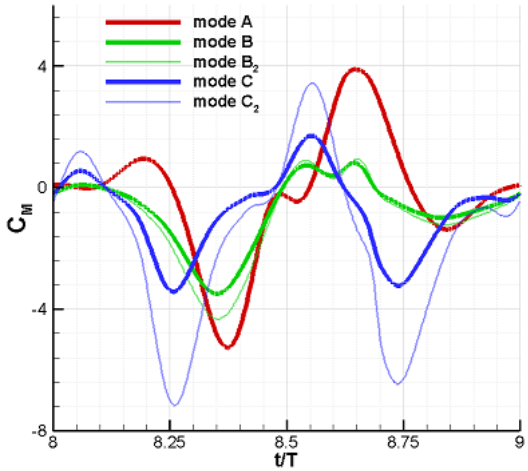

Figure 7: Time histories of C_m for all cases studied. The solid lines denote the cases at same Reynolds number of 1000. The dashed lines denote the cases with constant reduced frequency of 0.25.

The test cases “mode B_2” and “mode C_2” are also shown to represent the effects of Reynolds number to the “figure-of-eight” motion. The smaller viscous effect with increasing Reynolds number results in smaller vortex structures and greater peak values for hovering. The general trend for “mode B_2” and “mode C_2” are same with their

counterparts but with the increase of Reynolds number, the aerodynamic force's peak values are increasing. This general trend could also be investigated for normal hover mode to ensure about the effect of Reynolds number on hovering aerodynamics. The mean of the force coefficients for three hovering modes are given in Table 1. All figure of eight motions have a favorable effect on the lift coefficient.

	Mode A	**Mode B**	**Mode C**
Mean C_L	0.124	0.382	0.431
Mean C_D	0.010	-0.001	0.038

Figure 6: Mean force coefficients of three hovering motions at the same Reynolds number (Re=1000).

4 CONCLUSIONS

The effect of vertical translation on hovering aerodynamics is investigated numerically for constant Reynolds number and reduced frequency. The unsteady, laminar, incompressible Navier-Stokes equations are solved using a commercial pressure-based solver with dynamic mesh feature. Three different hovering modes are defined and the vortex-fields and instantaneous aerodynamic forces are visualized and compared. It is shown that with increasing Reynolds number for "figure-of-eight" motions, the aerodynamic force's peaks are also increasing.

REFERENCES

[1] Z. J. Wang, Vortex Shedding and Frequency Selection in Flapping Flight, *Journal of Fluid Mechanics*, **410**, pp. 323-341 (2000)

[2] K. C. Hall, S. A. Pigott and S. R. Hall, Power requirements for large amplitude flapping flight, *Journal of Aircraft* **35**, pp. 17-24 (1998)

[3] P. Freymuth, Thrust generation by an airfoil in hover modes, *Experiments in Fluids*, **9**, pp. 17-24 (1990)

[4] R. Knoller, Die Gesetze des Luftwiderstandes, *Flug- und Motortechnik (Wien*) **21**, pp.1- 7, 1909

[5] A. Betz, Ein beitrag zur Erklärung des Segelfluges, *Zeritschrift für Flugtechnik und Motorluftschiffahrt*, **3**, pp. 269-272, 1912

[6] U. Pesavento and Wang Z. J., Flapping wing flight can save aerodynamic power compared to steady flight, *Physical Review Letters* **103,** pp. 118102 (2009)

[7] F. O. Lehmann, The Mechanisms of Lift Enhancement in Insect Flight, *Naturwissenschaften* **91**, pp. 101-122, (2004)

[8] M. Platzer, K. D. Jones, J. Young and J. C. S. Lai, Flapping-wing aerodynamics: progress and challenges, *AIAA Journal* **46,** pp. 2136-2149 (2008)

[9] Z. J. Wang, Dissecting insect flight, *Annual Review of Fluid Mechanics* **37**, pp. 183-210 (2005)

[10] S. P. Sane, The aerodynamics of insect flight, *The Journal of Experimental Biology* **206**, 4191-4208 (2003)